Optical Metamagnetism and Negative-Index Metamaterials

Uday K. Chettiar, Shumin Xiao, Alexander V. Kildishev, Wenshan Cai, Hsiao-Kuan Yuan, Vladimir P. Drachev, and Vladimir M. Shalaev

Abstract

A new class of artificially structured materials called metamaterials makes it possible to achieve electromagnetic properties that do not exist in nature. In this article, we review the recent progress made in the area of optical metamaterials, specifically artificial magnetism and negative-index metamaterials. It was predicted that nanostructured metamaterials could provide magnetic responses and negative refractive indexes at optical frequencies. To date, optical metamagnetics have been fabricated to demonstrate magnetic responses in the infrared range and across the entire visible spectrum. Metamaterials showing negative refractive indexes, also called negative-index materials (NIMs), have also been demonstrated in the infrared range and at the border with the visible spectral range. Additionally, we report the results of a sample that displays NIM behavior for red light at a wavelength of 710 nm and another sample that displays double-negative NIM behavior at 725 nm. Both observations represent the shortest wavelengths so far at which NIM behavior has been observed for light. We also discuss the fabrication challenges and the impact of fabrication limitations, specifically the effect of surface roughness of the fabricated structures, on the optical properties of the metamaterials.

Introduction

The refractive index, n, is one of the most important optical characteristics of any material. It can be written as

$$n = n' + in'', \tag{1}$$

where n' is the real part and n'' is the imaginary part of the refractive index. The same convention is used throughout this article, where a single prime (′) denotes the real part and a double prime (″) denotes the imaginary part. Conventionally, the real part of the refractive index (n') is assumed to be positive, but a negative refractive index ($n' < 0$) does not violate any fundamental laws of physics. Negative-index materials (NIMs), with $n' < 0$, have some remarkable properties that make them candidates for a number of potential applications such as super-resolution.[1]

In a landmark work in 1968, Veselago showed that a material with simultaneous negative permeability ($\mu = \mu' + i\mu''$) and negative permittivity ($\varepsilon = \varepsilon' + i\varepsilon''$) has a negative refractive index.[2] However, this is actually a strong (sufficient) condition for a negative index. The necessary condition for a negative index is given by

$$\varepsilon'\mu'' + \mu'\varepsilon'' < 0. \tag{2}$$

Equation 2 strictly implies that $n' < 0$ cannot occur in a passive metamaterial with $\mu = 1 + 0i$. Consequently, a magnetic response is essential in a NIM. Unfortunately, there is no magnetic response in nature at optical frequencies; hence, to obtain an optical NIM, an artificial magnetic response must be achieved as a prerequisite.

Following from the previous discussion, two types of NIMs can be introduced. A double-negative NIM (DN-NIM) is a metamaterial with simultaneously negative real parts of the effective permeability and permittivity constants ($\mu' < 0$ and $\varepsilon' < 0$). A single-negative NIM (SN-NIM) has a negative refractive index with either $\mu' < 0$ or $\varepsilon' < 0$ (but not both). At optical wavelengths, obtaining $\varepsilon' < 0$ is easy compared to obtaining $\mu' < 0$, as noble metals naturally have a negative ε' value above the plasma wavelength.

The ratio $-n'/n''$ is often taken as a figure of merit (FOM) of NIMs because low-loss NIMs are desired. The FOM can be rewritten as

$$\text{FOM} = -(|\mu|\varepsilon' + |\varepsilon|\mu')/(|\mu|\varepsilon'' + |\varepsilon|\mu''), \tag{3}$$

indicating that a DN-NIM with $\mu' < 0$ and $\varepsilon' < 0$ is better than an SN-NIM with the same $n' < 0$ but with $\mu' > 0$, because a DN-NIM will have a lower n'' value than an SN-NIM with the same value of n'. In addition, DN-NIMs can provide better impedance matching than SN-NIMs.[3]

In this article, we review some of the work from our and other groups related to the demonstration of artificial magnetism and a negative index at optical frequencies. We specifically focus on our recent work on optical metamagnetics fabricated for the whole visible spectrum from red to blue.[4,5] We report our results demonstrating DN-NIM behavior close to 725 nm, which further decreases the wavelength at which DN-NIM behavior has been observed thus far.[3,6] In addition, we report SN-NIM behavior at 710 nm, which also decreases the wavelength at which a negative index for light has been observed.[7] For surface plasmon polaritons (SPPs), negative index behavior has also been demonstrated at shorter wavelengths in two-dimensional waveguides.[8] SPPs are the collective oscillations of electrons close to a metal surface that propagate along the metal surface.[9]

Metamagnetics

As stated in the preceding section, negative permeability and negative permittivity are needed to obtain a negative refractive index. Obtaining negative permittivity at optical frequencies is straightforward, as plasmonic materials exhibit negative permittivities at frequencies below the plasma frequency and common plasmonic materials such as gold and silver have plasma frequencies just above

the visible range. Unlike permittivity, however, the permeabilities of all naturally occurring materials are essentially equal to unity at optical frequencies. This is because the magnetic field couples very weakly to atoms as opposed to the electric field, which can interact strongly with atoms.

As a first step to achieving a negative refractive index, materials must be found that exhibit not only a nonunity value of permeability, but also, ideally, a negative permeability. It should be noted, however, that even materials with nonunity values of permeability are of immense importance and can find useful applications in such diverse areas as subwavelength waveguides and antennas,[10,11] filters,[12] and electromagnetic cloaking devices.[13] In conventional materials, only the electric field strongly interacts with the matter through the permittivity. In contrast, a nonunity value of permeability enables the magnetic field to interact with the material, and this increased flexibility makes it possible to achieve the mentioned applications just mentioned.

Various structures including bihelixes,[14] split-ring resonators (SRRs),[15] and pairs of metal nanorods[16–18] have been proposed for metamagnetics (artificial materials with magnetic response). Figure 1 shows a schematic of these three structures. A bihelix medium has also been realized experimentally.[14] The SRR geometry has been extensively used to demonstrate artificial magnetism from the microwave frequency range to near-infrared wavelengths up to 800 nm.[19,20] However, the feasibility of the SRR geometry in the optical range is restricted because of an inherent saturation effect that limits its magnetic response.[21] Therefore, in our work, we employed a nanostrip pair design to demonstrate artificial magnetic responses over the entire visible spectrum.[4,5] In the current state of art, the nanostrip pair design (conceptually similar to that in figure 1c) is the best option for achieving artificial magnetic response in the visible spectral range.

In this article, we consider a few examples of metamagnetic samples that show a negative permeability in the visible range[4,5] and also discuss the fabrication methods and challenges. Figure 2a shows a schematic cross section of a unit cell of the negative-permeability structure, which is a periodic array of pairs of silver strips, along with a scanning electron microscopy (SEM) image of the fabricated structure. Although the schematic shows the cross section to be rectangular in shape, the physical samples have a trapezoidal cross section because of limitations in fabrication. The structure was fabricated using electron beam lithography.[4] For the study, two samples (denoted as Samples A and B) with slightly different geometries and different silver surface roughness were fabricated. A negative effective permeability value was obtained using numerical simulations,[4] and the results are in good agreement with the transmission and reflection spectra obtained from optical measurements for each sample. The values of μ′ were about –1 in Sample A and about –1.7 in Sample B at wavelengths of 770 nm and 725 nm, respectively.

Figure 1. (a) Schematic of a bihelix structure. The gold helix is left-handed, and the silver helix is right-handed. The two helixes are shown in different colors to improve clarity. In a real device, both helixes are made using the same material. (b) Schematic of a pair of split-ring resonators. In the case of a single split-ring resonator, the inner resonator is missing. (c) Schematic of a pair of nanorods.

Electron beam lithography (EBL), which was used to fabricate Samples A and B, is one of the most preferred techniques used to fabricate nanoscale structures because of the high resolution and superior quality and control that it provides. Fabrication using EBL is usually performed on a conducting surface. This helps in dispersing away the electrons from the electron beam and consequently avoids charging effects. For optical structures, an indium tin oxide (ITO) coated glass substrate is used because ITO conducts electrons but behaves as a dielectric at visible wavelengths. The fabrication procedure also involves electron beam evaporation, which is used to produce a stack of lamellar films.

The deposition process is an important step, as it determines the quality of the final structures. For Samples A and B, the deposition process was optimized by fabricating a number of samples under different conditions; for example, the rate of deposition was varied from 80 Å/s to 0.5 Å/s to characterize the effects of deposition rate on the quality and optical properties of the final structure.

Atomic force microscopy (AFM) measurements of the root-mean square (rms) value of surface roughness indicated that a lower deposition rate of silver (0.5 Å/s, Sample B) resulted in lower surface roughness than a higher deposition rate

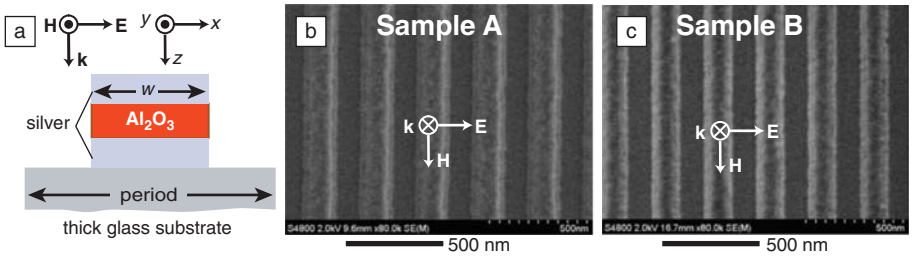

Figure 2. (a) Schematic of a single pair of nanostrips, where *w* represents the width of the nanostrips. The metamaterial consists of a periodic array of the nanostrip pairs. The transverse magnetic (TM) polarization is depicted in the figure. The transverse electric (TE) polarization is orthogonal to the TM polarization. **H**, **E**, and **k** represent the directions of the magnetic field, electric field, and wave propagation for TM polarization. *x*, *y*, and *z* represent the coordinate axes. (b), (c) Scanning electron microscopy (SEM) images of Samples A and B, respectively. Sample A was fabricated using a high deposition rate (2 Å/s), whereas Sample B was fabricated using a low deposition rate (0.5 Å/s). The SEM images also include the directions of the fields for TM polarization. The real samples have a trapezoidal cross section as opposed to the ideal rectangular cross section shown in the schematic. (Adapted from Reference 4.)

(~2 Å/s, Sample A). Note that, for a typical deposition procedure, the rate cannot be set lower than 2 Å/s, as the deposition of silver heats the resist material and makes the lift-off process impossible. To cool the resist, we performed a four-step deposition process with 10-min pauses between each deposition step. This new procedure allowed for the use of a lower deposition rate of about 0.5 Å/s to obtain a lower surface roughness while ensuring successful lift-off, providing an overall better quality sample. The vertical layer structures of the films from the ITO-coated glass were as follows: Sample A consisted of 10 nm of alumina, 30 nm of silver, 40 nm of alumina, 30 nm of silver, and 10 nm of alumina. In the case of Sample B, the two layers of silver were 35 nm thick. Representative SEM images of the fabricated structures of Samples A and B are shown in Figures 2b and 2c, respectively. From the SEM images, one can see that Sample A shows higher roughness than Sample B. A more quantitative comparison is provided by the AFM scans as described later in this section.

The samples can be characterized by the transmission and reflection spectra. Because the structures are inherently anisotropic, the spectra should be measured for different polarizations using linearly polarized light. In the case of the nanostrip sample, the two different polarizations are termed transverse electric (TE) and transverse magnetic (TM) polarizations. For TE polarization, the electric field of the incident light is linearly polarized parallel to the length of the silver strips, whereas in TM mode, the electric field is rotated by 90° relative to the TE case. Figure 2 depicts TM polarization.

Figures 3a and 3b show transmission and reflection spectra obtained from the optical measurements of Samples A and B, respectively, for TM polarization at normal incidence along with the simulated results. Figures 3c and 3d show the real parts of the obtained effective permeabilities and permittivities for Samples A and B, respectively. Samples A and B show permeabilities of –1 and –1.7 at 770 nm and 725 nm, respectively. In TE polarization, both samples act as "diluted metal" films without any resonant response.[4]

It has been shown that roughness in the nanostrip structures along with finite-size effects result in a decreased negative permeability because of additional losses caused by increased electron scattering.[22] Negative permeability is achieved through a resonant response, and the increased losses due to roughness decrease the quality factor of the magnetic resonance. In this case, these effects result in a decreased negative permeability relative to the ideal case (with no roughness) by a factor of 7.8 for Sample A and by a factor of only 2.4 for Sample B, which has better surface quality.[4] These results are consistent with the statistical analysis of surface roughness obtained from AFM scans. The example cross sections of the AFM images shown in Figures 4a and 4b for Samples A and B, respectively, indicate substantial differences in the surface roughness of the samples. Sample A is characterized by larger variations in rms roughness across different regions ranging from 2 nm to 6 nm (versus 1.5–2.5-nm variations for Sample B), with an rms roughness value over the total area of about 3.7 nm (versus 2 nm for Sample B), which explains the better magnetic response from Sample B.

In summary, there are substantial deviations from the ideal, smooth silver strip surface, and these deviations result in enhanced absorption at the resonances that were observed experimentally in the resonant plasmonic elements of the nanostructured samples. These nonidealities and the resulting deviations from the ideal properties can be reduced by improving the fabrication methods to minimize the imperfections. It is observed that using slower deposition decreases the surface roughness and gives improved magnetic response.

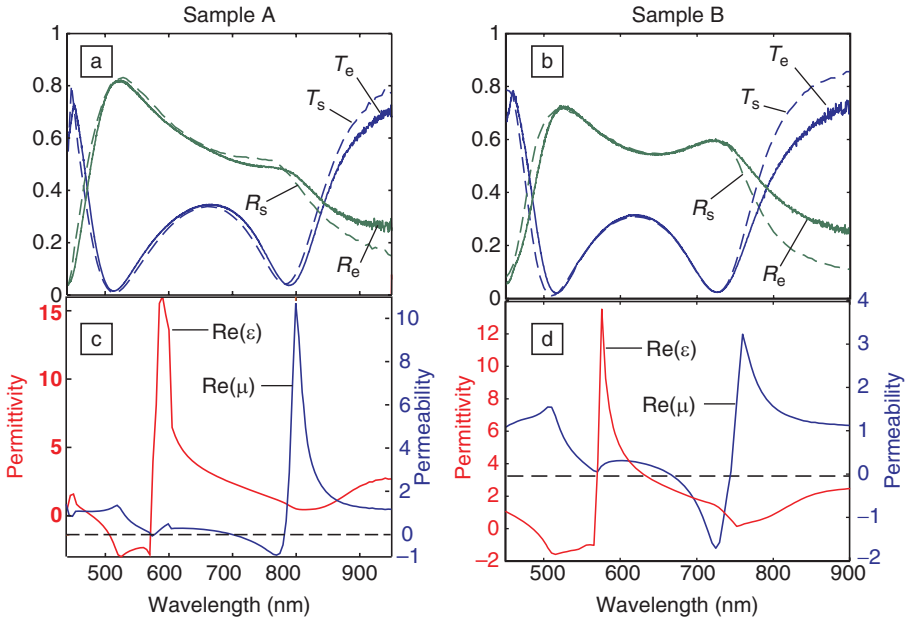

Figure 3. (a), (b) Transmission and reflection spectra of Samples A and B, respectively. Solid lines and subscript e represent experimental data, and dashed lines and subscript s represent simulated data. *T* is transmittance, and *R* is reflectance. (c), (d) Real parts of the obtained effective permeabilities (μ) and permittivities (ε) for Samples A and B, respectively. (Adapted from Reference 4.) Note that Sample B has a stronger magnetic response as is evident for the more negative value of permittivity at the magnetic resonance.

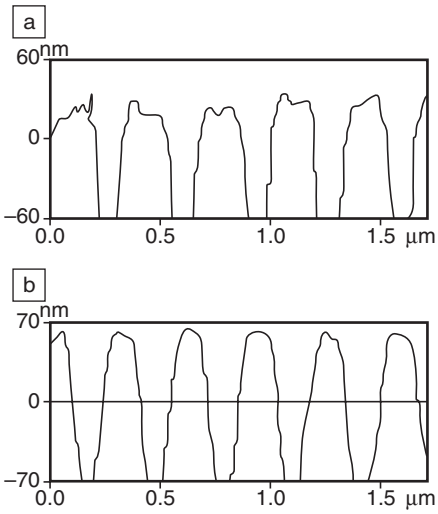

Figure 4. Representative atomic force microscopy cross sections showing surface roughness of (a) Sample A and (b) Sample B. (Reproduced with permission from Reference 4. Copyright 2007 Optical Society of America.) Sample A, which was fabricated using a higher deposition rate, shows higher roughness as compared to Sample B. This implies that a lower deposition rate results in a lower roughness.

Extension of Metamagnetism to the Entire Visible Spectrum

The results described in the preceding section were later extended by fabricating a family of nanostrip pairs with a range of widths to provide magnetic resonance across the visible spectrum.[5] Figure 5 shows optical microscope images of the arrays of samples for TE and TM polarization in reflection and transmission modes. Each sample is 160 μm × 160 μm in size. For resonant TM polarization, distinct colors can be observed in the different samples in both transmission and reflection modes, indicating a unique resonant frequency in each sample. On the other hand, for nonresonant TE polarization, the colors are the same for all of the samples. In this case, the samples act as "diluted metal" films with more reflection and less transmission at longer wavelengths. This shows that the samples exhibit a resonant response for TM polarization with a strong dependence on the geometry, whereas there is no resonant response for TE polarization and the samples simply behave as thin metal films.

The metamagnetic samples were optically characterized to obtain their spectral responses.[5] Figures 6a and 6b show the transmission and reflection spectra of the six samples in TM polarization. Strong resonant behavior can be seen in all of the samples for wavelengths ranging from 491 nm to 754 nm, covering the majority of the visible spectrum. The position of the magnetic resonance moves towards shorter wavelengths as the width of the nanostrip pairs decreases. Figure 6c shows the real part of permeability for the six samples as a function of the resonance wavelengths. The permeability ranges from –1.6 at 750 nm to 0.5 at 500 nm.

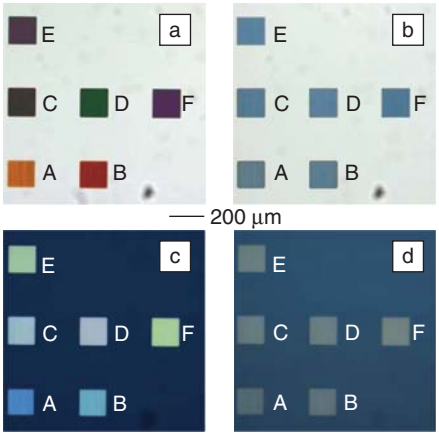

Figure 5. Optical microscope image of an array of magnetic samples for two orthogonal polarizations. Each sample is 160 μm × 160 μm. (a) Transmission mode with TM polarization, (b) transmission mode with TE polarization, (c) reflection mode with TM polarization, (d) reflection mode with TE polarization. (Reproduced with permission from Reference 5. Copyright 2007 Optical Society of America.)

Negative-Index Metamaterials

As described in the preceding section, an array of metal nanostrip pairs can exhibit a negative permeability. A modification of this structure, sometimes known as a double-grating or fishnet structure, is widely used to demonstrate negative indexes at optical frequencies. A fishnet structure is essentially a combination of two nanostrip pair structures that are orthogonal to each other. An example SEM image of a fishnet structure is shown in Figure 7a. This structure has been used to demonstrate NIM behavior at 780 nm,[6] 1.5 μm,[23] and 2 μm.[24] However, in all of these cases, only SN-NIM behavior was observed.

The first DN-NIMs in the optical range were demonstrated at 1.4 μm with an FOM of about 3[25] and at 1.8 μm with an FOM above 1.[26] Most recently, the wavelength at which DN-NIM behavior has been observed was reduced to about 810 nm with an FOM of 1.3.[3] For a different polarization, the same sample also demonstrated SN-NIM behavior close to 770 nm with an FOM of 0.7. Later, the shortest wavelength at which DN-NIM behavior has been observed to date (excluding SPPs in two-dimensional waveguides) was reduced further to 725 nm with an FOM of 1.05,[7] which further decreases the earlier reported wavelength.[3] The shortest wavelength at which NIM behavior has been observed has also been reduced to 710 nm, with an SN-NIM sample showing an FOM of 0.5,[7] also an

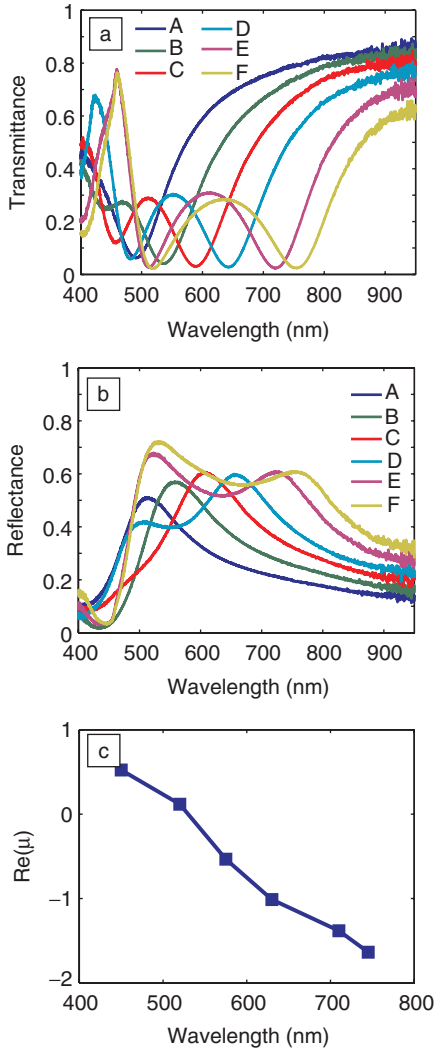

Figure 6. (a) Transmission and (b) reflection spectra for the array of magnetic samples. (c) Real part of the permeability (μ) as a function of the resonance wavelength for the six samples in the array of magnetic samples. (Reproduced with permission from Reference 5. Copyright 2007 Optical Society of America.)

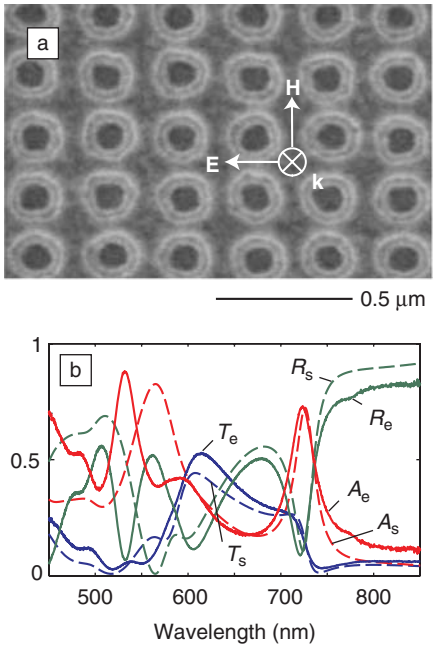

Figure 7. (a) SEM image and (b) experimental and simulated spectra of a double-negative negative-index material (DN-NIM) sample. **H, E,** and **k** define the directions of the magnetic field, electric field, and wave propagation, respectively. *T* is transmittance, *R* is reflectance, and *A* is absorbance, with solid lines and subscript e representing experimental data and dashed lines and subscript s representing simulated data. (See Reference 7.)

improvement in comparison with the earlier work.[3]

The structure was fabricated using a procedure similar to that described previously for fabricating the magnetic samples.[3] In the fabrication process, a low deposition rate was used to minimize the roughness of the metal surface. The structures were characterized by measuring the spectral response. Figure 7a shows an SEM image of the sample, and Figure 7b shows simulated and experimental spectra of the sample.[7]

The experimental and simulated spectra shown in Figure 7b demonstrate a good match over a broad range of measured wavelengths (from 600 nm to 850 nm) and include sharp resonance features around 550 nm and 720 nm. The experimental and simulation results do not agree as well at shorter wavelengths because of the uncertainty in the properties of silver at such small dimensions. We used the properties of bulk silver in our simulations,[27] with the relaxation constant multiplied by 3 to account for additional losses.[3] However, the permittivity of silver shows larger deviations from the tabulated data at shorter wavelengths because of the presence of interband transitions. Nevertheless, the agreement is excellent above 600 nm, which includes the important region of DN-NIM behavior.

The simulations demonstrate the origin of the two main resonances around 550 nm and 720 nm as shown in Figure 8. Figure 8a shows a schematic of a unit cell of the fishnet structure. The region marked with red lines is the area that is responsible for the resonances. Figures 8b and 8c depict the field maps of the highlighted region at 540 nm and 720 nm, respectively, obtained from the simulations. The absorbance spectrum exhibits strong resonant behavior at these two wavelengths. In the field maps, the color map represents the magnetic field, which is normalized with respect to the incident magnetic field. The arrows represent the electric displacement. In Figure 8b, one can see that the electric displacements in both the top and bottom metal strips are aligned together, resulting in a strong electric dipole response, which implies a resonance that is electrical in nature. In Figure 8c, the electric displacements in the two metal strips are oppositely directed, resulting in a magnetic dipole moment that is evident from the strong magnetic field between the two strips. Hence, this resonance is termed a magnetic resonance. It is worth noting that the magnetic field in the dielectric space is negative with respect to the incident field, resulting in a negative permeability.

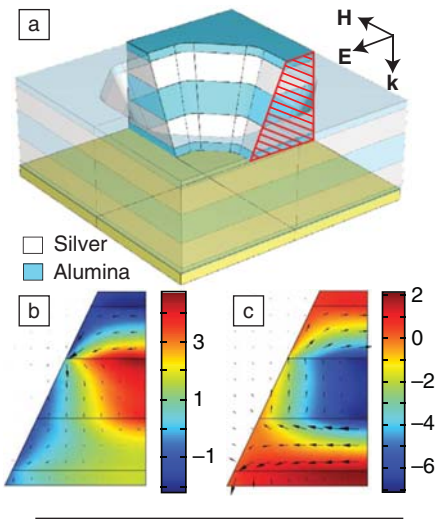

Figure 8. (a) Schematic figure of a unit cell of the fishnet structure along with the incident polarization. **H, E,** and **k** define the directions of the magnetic field, electric field, and wave propagation, respectively. The fishnet structure consists of three layers of alumina separated by two layers of silver. The region highlighted with the red lines is the region of resonance. (b), (c) Field maps of the region highlighted in (a) at wavelengths of 540 nm and 720 nm, respectively. The color represents the magnetic field normalized with respect to the incident magnetic field, and the arrows represent the electric displacement.

The results obtained for the sample are shown in Figure 9.[7] These results are an improvement over the previously reported results.[3] The real part of the refractive index (n') and the figure of merit (FOM = $-n'/n''$) are depicted in Figure 9a. For the sake of clarity, the FOM is set to zero for $n' > 0$. The best FOM of 1.05 is obtained at a wavelength of 725 nm, where n' is about –0.8. The minimum value of the refractive index, $n' \approx -1.2$, is achieved at 735 nm, but with a lower FOM of 0.7. As indicated in Figure 9b, μ' is negative between 720 nm and 730 nm. This band represents the DN-NIM regime. Because the negative permeability is obtained through a resonant response, the bandwidth is limited by the resonance bandwidth. This is a common limitation in structures that rely on resonant responses. In principle, the bandwidth could be increased by using a mixture of geometries that resonate at different wavelengths, but the practical realization is limited because of coupling effects between the different geometries and also a weakened cumulative response due to a reduced density of the individual geometries.

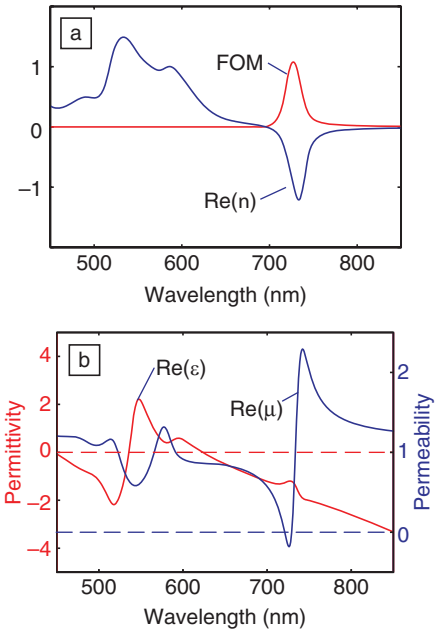

Figure 9. (a) Real part of refractive index (n) and figure of merit (FOM) for a sample of a DN-NIM. (b) Real parts of the permittivity (ε) and permeability (μ) for the DN-NIM sample. (See Reference 7.)

The shortest wavelength at which SN-NIM behavior has been observed was also reduced further[7] in comparison with the earlier reported results.[3] An SEM image of this sample is shown in Figure 10a, and the simulated and experimental spectra are shown in Figure 10b. One can clearly see the strong resonant response around 710 nm. There is also good agreement between the experimental and simulated results. The simulated results were used to obtain the effective refractive index for the sample and are shown in Figure 10c. The structure shows a maximum FOM of 0.5 at 710 nm with $n' \approx -0.6$.

Conclusions

Metamaterials have the potential of adding another dimension to the set of existing materials by providing novel properties that do not exist in nature. Optical metamagnetics and negative-index metamaterials are two such examples. Optical metamagnetics allow magnetic responses to be obtained in the infrared range and across the entire visible spectrum even though no natural material exhibits magnetic behavior at these frequencies. Optical metamagnetics make it possible to achieve several applications that are not possible or would be difficult

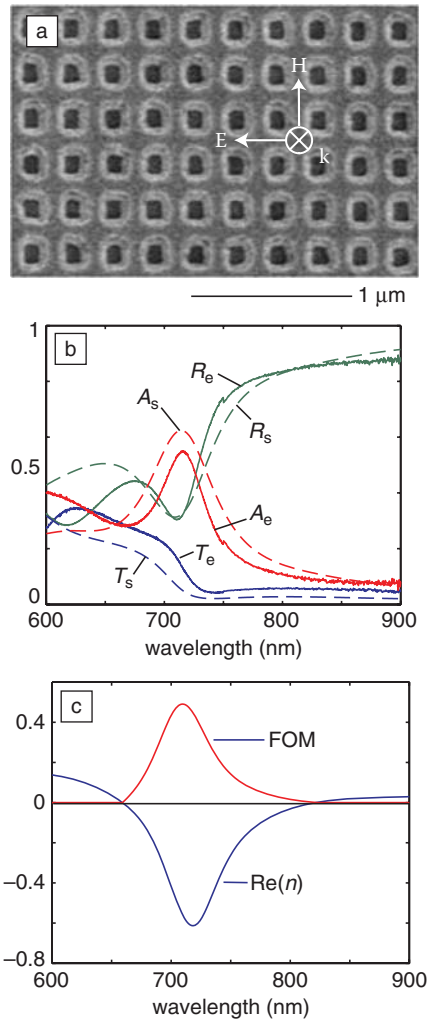

Figure 10. (a) SEM image of a sample of a single-negative negative-index material (SN-NIM) and (b) experimental and simulated spectra of the SN-NIM sample. In (a), **H**, **E**, and **k** define the directions of the magnetic field, electric field, and wave propagation, respectively. In (b), *T* is transmittance, *R* is reflectance, and *A* is absorbance, with solid lines and subscript e representing experimental data and dashed lines and subscript s representing simulated data. (c) Real part of the refractive index (*n*) and figure of merit (FOM) for the SN-NIM sample. (See Reference 7.)

without a magnetic response such as subwavelength waveguides and antennas, filters, electromagnetic cloaking devices, and negative-refractive-index materials.

Negative refractive indexes have been demonstrated at optical wavelengths using various geometries such as paired nanorod arrays and fishnets. Of these, the fishnet geometry shows more promise, and it has been used to demonstrate DN-NIM behavior at wavelengths as short as 725 nm.[7] The sample showed a maximum figure of merit of 1.05 with $n' \approx -0.8$. The shortest wavelength at which NIM behavior has been observed is 710 nm for a sample displaying an SN-NIM response with a maximum FOM of 0.5 with $n' \approx -0.6$. The next challenge faced by the community is to achieve NIM behavior throughout the visible range with an acceptable figure of merit. This is a difficult problem, as metals such as gold and silver show progressively greater losses as the wavelength decreases. Loss compensation through active gain materials has been suggested as a means to overcome this hurdle and achieve superior NIM performance at visible wavelengths.[28]

The quality of the nanostructured metal in metamagnetics and NIMs can have a substantial impact on their performance. Through the use of optimized fabrication procedures, there is significant room for improving metamaterial properties. For example, use of a lower deposition rate would allow the surface roughness of the structures to be reduced, resulting in a much better response. As the field of metamaterials continues to grow and expand, we anticipate a variety of unique and exciting applications in optics based on this new class of materials.

Acknowledgments

This work was supported by ARO-MURI Award 50342-PH-MUR and NSF-PREM Grant DMR-0611430.

References

1. J.B. Pendry, *Phys. Rev. Lett*. **85**, 3966 (2000).
2. V.G. Veselago, *Sov. Phys. Usp*. **10**, 509 (1968).
3. U.K. Chettiar, A.V. Kildishev, H.K. Yuan, W.S. Cai, S.M. Xiao, V.P. Drachev, V.M. Shalaev, *Opt. Lett*. **32**, 1671 (2007).
4. H.K. Yuan, U.K. Chettiar, W.S. Cai, A.V. Kildishev, A. Boltasseva, V.P. Drachev, V.M. Shalaev, *Opt. Express* **15**, 1076 (2007); available at http://www.opticsinfobase.org/abstract.cfm?URI=oe-15-3-1076.
5. W.S. Cai, U.K. Chettiar, H.K. Yuan, V.C. de Silva, A.V. Kildishev, V.P. Drachev, V.M. Shalaev, *Opt. Express* **15**, 3333 (2007); available at http://www.opticsinfobase.org/abstract.cfm?URI=oe-15-6-3333.
6. G. Dolling, M. Wegener, C.M. Soukoulis, S. Linden, *Opt. Lett*. **32**, 53 (2007).
7. V.M. Shalaev, W. Cai, U.K. Chettiar, H.K. Yuan, A.V. Kildishev, V.P. Drachev, paper presented at SPIE Optics + Photonics, San Diego, CA, 10 August 2008.
8. H.J. Lezec, J.A. Dionne, H.A. Atwater, *Science* **316**, 430 (2007).
9. H. Raether, *Surface Plasmons on Smooth and Rough Surfaces and on Gratings*; Springer Tracts in Modern Physics (Springer-Verlag, New York, 1988), p. 136.
10. P.A. Belov, C.R. Simovski, *Phys. Rev. E* **72**, 036618 (2005).
11. A. Ourir, A. de Lustrac, J.M. Lourtioz, *Appl. Phys. Lett*. **88**, 084103 (2006).
12. V.A. Fedotov, P.L. Mladyonov, S.L. Prosvirnin, N.I. Zheludev, *Phys. Rev. E* **72**, 056613 (2005).
13. J.B. Pendry, D. Schurig, D.R. Smith, *Science* **312**, 1780 (2006).
14. A.N. Lagarkov, V.N. Semenenko, V.A. Chistyaev, D.E. Ryabov, S.A. Tretyakov, C.R. Simovski, *Electromagnetics* **17**, 213 (1997).
15. J.B. Pendry, A.J. Holden, D.J. Robbins, W.J. Stewart, *IEEE Trans. Microwave Theory Technol*. **47**, 2075 (1999).
16. A.N. Lagarkov, A.K. Sarychev, *Phys. Rev. B* **53**, 6318 (1996).
17. V.A. Podolskiy, A.K. Sarychev, V.M. Shalaev, *J. Nonlinear Opt. Phys. Mater*. **11**, 65 (2002).
18. V.A. Podolskiy, A.K. Sarychev, V.M. Shalaev, *Opt. Express* **11**, 735 (2003); available at http://www.opticsexpress.org/abstract.cfm?uri=oe-11-7-735.
19. D.R. Smith, W.J. Padilla, D.C. Vier, S.C. Nemat-Nasser, S. Schultz, *Phys. Rev. Lett*. **84**, 4184 (2000).
20. C. Enkrich, M. Wegener, S. Linden, S. Burger, L. Zschiedrich, F. Schmidt, J.F. Zhou, T. Koschny, C.M. Soukoulis, *Phys. Rev. Lett*. **95**, 203901 (2005).
21. M.W. Klein, C. Enkrich, M. Wegener, C.M. Soukoulis, S. Linden, *Opt. Lett*. **31**, 1259 (2006).
22. V.P. Drachev, U.K. Chettiar, A.V. Kildishev, H.K. Yuan, W.S. Cai, V.M. Shalaev, *Opt. Express* **16**, 1186 (2008). http://www.opticsinfobase.org/abstract.cfm?URI=oe-16-2-1186
23. V.M. Shalaev, W. Cai, U.K. Chettiar, H.K. Yuan, A.K. Sarychev, V.P. Drachev, A.V. Kildishev, *Opt. Lett*. **30**, 3356 (2005).
24. S. Zhang, W.J. Fan, N.C. Panoiu, K.J. Malloy, R.M. Osgood, S.R.J. Brueck, *Phys. Rev. Lett*. **95**, 137404 (2005).
25. G. Dolling, C. Enkrich, M. Wegener, C.M. Soukoulis, S. Linden, *Opt. Lett*. **31**, 1800 (2006).
26. S. Zhang, W.J. Fan, K.J. Malloy, S.R.J. Brueck, N.C. Panoiu, R.O. Osgood, *J. Opt. Soc. Am. B* **23**, 434 (2006).
27. P.B. Johnson, R.W. Christy, *Phys. Rev. B* **6**, 4370 (1972).
28. T.A. Klar, A.V. Kildishev, V.P. Drachev, V.M. Shalaev, *IEEE J. Sel. Top. Quantum Electron*. **12**, 1106 (2006). □